BMC Genomics

RESEARCH

Open Access

The whole genome analysis of the wild-type and attenuated orf virus reveals that ORF022 facilitates viral replication

Tian Jing[1†], Yunpeng Wang[1†], Yukun Bu[1], Xi Chen[1], Shutong Feng[1], Wenbo Liu[1], Zhannur Niyazbekova[2], Dekun Chen[1], Xiaolong Gao[3*] and Wentao Ma[1*]

Abstract

Background Contagious ecthyma is an acute infectious zoonosis caused by orf virus (ORFV). Live-attenuated ORFV vaccines have played a crucial role in preventing contagious ecthyma for decades. However, these vaccines often fail to induce long-lasting immunity. In recent years, numerous ORFV genome sequences have been published, yet genomic data for attenuated strains remain limited. Furthermore, no comprehensive whole-genome-based single nucleotide polymorphisms (SNPs) analysis has been conducted to compare ORFV wild-type and attenuated strains.

Results In this study, we performed whole-genome sequencing of ORFV wild-type and attenuated strains from Shaanxi Province. We identified two ORFV strains with genomes shorter than 130 kb, which are closely related to the SC1 attenuated strain from Sichuan Province. Additionally, we noticed that 24 genes in the attenuated strain had SNPs, with the highest number of mutations occurring in the ORF022 gene. The function of the ORF022 gene has not been previously reported. Through in vitro experiments, we demonstrated that overexpression of ORF022 enhances ORFV replication in cells. The RNA-sequencing analysis revealed that ORF022 modulates host inflammation-related signaling pathways, as evidenced by the suppression of TNF, IL-17, and Toll-like receptor signaling pathways.

Conclusions Our findings suggest that the ORF022 in ORFV wild-type strain inhibits the host inflammatory response, reduces the immune response to ORFV, and facilitates viral replication. SNP events in attenuated strains (aFX0910) are one of the reasons for its attenuation. Investigations into the genomic sequences of attenuated viruses and the functional impact of mutated genes provide valuable insights into the mechanisms underlying ORFV attenuation and offer a foundation for the development of more effective ORFV vaccines.

Keywords Orf virus, Attenuated vaccines, Whole genome sequencing, Single nucleotide polymorphisms, RNA-sequencing

†Tian Jing and Yunpeng Wang contributed equally to this work.

*Correspondence:
Xiaolong Gao
gaoxiaolong1017@163.com
Wentao Ma
mawentao@nwafu.edu.cn

[1]College of Veterinary Medicine, Northwest A&F University, Yangling, Shaanxi Province 712100, China
[2]College of Animal Science and Technology, Northwest A&F University, Yangling, Shaanxi Province 712100, China
[3]College of Agriculture and Animal Husbandry, Qinghai University, Qinghai Province 810016 Xining, China

Background

Contagious ecthyma (CE), also known as Orf, is a zoonotic infectious disease characterized by epithelial lesions and caused by the Orf virus (ORFV). CE has been widely reported worldwide [1], with developing countries such as China and India identified as the predominant regions for ORFV infections [2, 3]. ORFV primarily infects sheep and goats but can also transmit to humans and other species [4–7]. While infected adult animals typically exhibit low mortality and high morbidity, the sheep industry suffers significant economic losses due to high mortality rates in lambs [8]. Vaccination with live attenuated vaccines is the primary strategy for CE control, but the mechanism of immune protection remains unclear, hindering the development of an effective vaccine [9]. A deeper understanding of attenuated vaccine mechanisms and the mutational events is essential for the development of novel ORFV vaccines.

In our previous study [10], we isolated a wild-type ORFV strain (FX0910) from Shaanxi Province and generated attenuated strains (aFX0910) through continuous cell passage. Compared to FX0910, aFX0910 exhibited a delayed cytopathic effect and induced milder pathological lesions in the lips of infected animals. Transcriptomics analyses revealed that aFX0910 downregulated host innate immune response. Single nucleotide polymorphism (SNP) analysis demonstrated amino acid mutations in both FX0910 and aFX0910 relative to the reference genome (SA00). However, these studies were based on transcription levels, and the sequence differences between FX0910 and aFX0910 remain uncharacterized for ORFV as a DNA virus.

The ORFV genome consists of double-stranded DNA spanning approximately 138–140 kb, with a G + C content of 64% and 130 putative genes [11]. While numerous ORFV genome sequences have been published in NCBI (Table S1), genomic data for attenuated strains remain scarce. The SC1 strain, obtained through serial in vitro passage of the SC strain, displays sequence variations in ORF007, ORF020, and ORF112 genes that likely contribute to its attenuated phenotype [12]. SNP represents a fundamental and widespread mechanism of viral evolution in nature [13, 14], with insertions and deletions (INDELs) constituting another common mutation type. Currently, no comprehensive whole-genome SNP analysis comparing ORFV wild-type and attenuated strains has been conducted. Characterizing the SNP events during viral passaging in vitro could provide critical insights into viral attenuation mechanisms.

Elucidating sequence differences between wild-type and attenuated strains is fundamental to investigating viral attenuation mechanisms. In this study, we performed whole genome sequencing (WGS) to obtain sequence information of both FX0910 and aFX0910, followed by genomic and SNP analyses. Our results provided genome-wide information of ORFV strains from Shaanxi Province, identifying 103 attenuation-associated SNP events. Notably, ORF022, the gene with the highest number of mutations, was functionally validated to both enhance viral replication and suppress host inflammatory responses, establishing its pivotal role in attenuation. In conclusion, our study elucidates the protective mechanism of attenuated ORFV strains at the genomic level and provides insights for selecting targets in novel engineering vaccines.

Materials and methods

Cell culture, viruses, and infection

The ORFV wild-type strain (FX0910) was isolated from Shaanxi Province, and the attenuated strain (aFX0910) was obtained by continuous cell passage. The primary goat lip fibroblasts (GLF) and ORFV strains used in this study were kindly provided by Dr. Xiaoting Yao. GLF culture, virus isolation and amplification were conducted following the previously established protocols [10]. GLF were infected with FX0910 or aFX0910 (500 µl of each). After incubation at 37 °C for 1 h, the viral suspension was removed and the cells were further incubated in minimum essential medium (ExCell Bio) supplemented with 2% fetal bovine serum (ExCell Bio).

DNA extraction, library construction, and sequencing

Upon observation of cytopathic effect (CPE) in all cells, they were collected using trypsin (Thermo Fisher Scientific) and DNA was extracted using the TIANamp Genomic DNA Kit. Subsequently, 1 µg genomic DNA was digested using EcoRI (NEB), and enzyme Purification product was interrupted by ultrasound. Following this, DNA fragments of 200 ~ 400 bp were selected by agarose electrophoresis and purified using QIAquick PCR Purification Kit. DNA terminal repair was performed through exonuclease, polymerase, and phosphokinase treatment. After purification using Agencourt AMpure XP magnetic beads, the 3 'terminal addition 'A' buffer reaction system was added. Subsequently, the final DNA library was constructed by Polymerase Chain Reaction (PCR) using a ligation buffer and double-strand sequencing adapters, with purification of the products carried out using the AMPure XP system (Beverly, USA). The quality of the libraries was assessed on the Agilent 5400 system (Agilent, USA) and quantified by real-time PCR (qPCR) to a concentration of 1.5 nM. Qualified libraries were pooled and sequenced on Illumina platforms using PE150 strategy (Novogene, Co., Ltd., China), in accordance with the effective library concentration and required data amount.

Mapping, assembly and SNPs analysis of whole genome data

The raw reads were cleaned using Trimmomatic-0.39 [15] to remove adapters, undetermined bases, and low-quality base reads. Then, the quality of clean reads was verified using FastQC-0.11.9 (https://github.com/s-andrews/FastQC). Virus reads were extracted by mapping them to the ORFV reference genome (RefSeq assembly accession: NC_005336.1) using BWA's mem algorithm and filtered using the Samtools view command [16]. The sequences were then assembled and annotated using Megahit-1.2.9 [17] and Liftoff [18], respectively. The complete genome sequences of FX0910 and aFX0910 have been submitted to GenBank with accession numbers PP943426 and PP943427. The genome of the FX strains was mapped using Geneious Prime software (https://www.geneious.com/features/prime), sequencing depth and coverage were calculated using BEDtools [19] and visualized using circlize [20]. Using FX0910 as the reference sequence, a pileup file was generated with the mpileup command in Samtools to identify mutation events in the FX0910 strain. The pileup files were annotated using SnpEff [21], and SNP visualization was performed using circlize and the ggplot2 package.

Phylogenetic analysis and ORF022 gene bioinformatics prediction

Multiple sequence alignment of FX0910 and aFX0910 with published ORFV sequences in NCBI was performed using MAFFT [22]. Bayesian phylogenetic trees were constructed using Bayesian evolutionary analysis by MrBayes-3.2.7 [23]. The parameters were set as follows: mcmc ngen = 1,000,000 samplefreq = 500 printfreq = 1000 diagnfreq = 5000, until the standard deviation of split frequencies is less than 0.01. The resulting tree files were visualized with iTOL (https://itol.embl.de/). Sequences homologous to ORF022 in paracoxvirus were collected for phylogenetic analysis of both nucleotide and amino acid sequences. Multiple sequence alignment files were analyzed for sequence identity using BioEdit (https://thalljiscience.github.io/), and the results were visualized using the pheatmap function. Bioinformatics prediction of ORF022 based on its amino acid sequence was conducted, focusing on secondary structure (SOPMA), tertiary structure (I-TASSER), phosphorylation modification site (DTU Health Tech-NetOGlyc-1.0). Finally, 3D structure visualization of proteins was performed using UCSF chimera [24].

ORF022 gene subcellular localization

To evaluate the subcellular localization of the ORF022 protein, the ORF022 gene was amplified using FX0910 and aFX0910 genomes as templates, respectively, and then cloned into the pEGFP-C1 vector (pEGFP-022 and pEGFP-a022). FX0910-ORF022 was also cloned to pcDNA3.1 plasmid (pcDNA3.1-022). GLF were either mock-infected or transfected with pEGFP-022 (or pEGFP-a022) and harvested at 24 h post-infection (hpi). Cell samples were fixed with 4% paraformaldehyde for 30 min, followed by permeabilization with Triton X-100 for 15 min after PBS washing. After three additional PBS washes, nuclear fluorescence staining was performed using 4′, 6-diamidino-2-phenylindole (DAPI) at 37℃ for 5 min. Finally, the cells were washed and observed under an inverted fluorescent microscope (Axio Observer, ZEISS, Germany).

ORF022 gene transcription dynamics

The dynamics of ORF022 mRNA and the copy number of ORF022 and ORFV were determined by real-time PCR. GLF were either mock infected or infected with FX0910/aFX0910 and harvested at 12, 24, 48 and 72 h. Infections were conducted with 10 μl of viral solution per 10^6 cells, with $TCID_{50}$ values for FX0910 and aFX0910 is $10^{-8.5}$ [10]. In addition, the mRNA levels of ORF019 and ORF027 were measured in parallel controls (2, 4, 6, 12 and 24 hpi). The mRNA and copy number of ORFV were detected with the B2L gene. The real-time PCR primers used for the specific detection of B2L, ORF022, ORFV019, and ORFV027 are listed in Table S2. The standard curve for ORF022 was constructed, and the copy number was calculated (Fig. S2D). The copy number of ORFV were determined based on the constructed standard curve [2]. The relative expression levels of the target genes, normalized to β-actin, were calculated by the $2^{-\Delta\Delta Ct}$ method.

ORF022 overexpression experiment

To explore the effect of ORF022 protein on ORFV, GLF were either mock-infected or transfected with pEGFP-022 (Seven HighTrans™ DNA non-liposome transfection reagent, transfected 400 ng plasmid per 10^5 cells) for 24 h and then infected with FX0910 (Infections were conducted with 10 μl of viral solution per 10^6 cells). The cells were harvested at 24 h post-transfection with FX0910, and DNA and RNA were extracted for real-time PCR analysis of mRNA and copy number of ORFV. The relative expression levels of the target genes, normalized to β-actin, were calculated by the $2^{-\Delta\Delta Ct}$ method. The aFX0910-ORF022 overexpression experiment followed the same protocol, with the plasmid used being pEGFP-a022 and the virus being aFX0910.

ORF022 interference experiment

Three pairs of small interfering RNA (siRNA) targeting ORF022, along with a negative control siRNA, were designed and synthesized by Tsingke (Beijing, China). All primers are listed in Table S2. GLF were infected

with FX0910 for 2 h and then transfected with either negative siRNA or ORF022 siRNA (Vazyme Lipomaster 3000 Transfection Reagent) The cells were harvested at 48 hpi and DNA and RNA were extracted for real-time PCR analysis of mRNA and copy number of ORF022 and ORFV. The relative expression levels of the target genes, normalized to β-actin, were calculated using the $2^{-\Delta\Delta Ct}$ method. The aFX0910-ORF022 interference experiment followed the same protocol, with the same siRNA and the virus being aFX0910.

Immunofluorescence analysis

GLF were transfected with pcDNA3.1-022 for 24 h and then infected with FX0910 for 24 h. Additionally, GLF were infected with FX0910 for 2 h and then transfected with either negative siRNA or ORF022 siRNA. Infections were conducted with 10 μl of viral solution per 10^6 cells, and three biological replicates were included for each treatment. Cells were subsequently subjected to immunofluorescence experiments and analyzed [2]. Integrated Optical Density (IOD) analysis of the immunofluorescence signals was performed using ImageJ software (https://imagej.net/ij/).

50% tissue culture infectious dose ($TCID_{50}$) assay

We collected cell supernatants from experiments involving ORF022 overexpression and interference. Virus titers were determined through $TCID_{50}$ assays [25] and calculated using the Reed-Muench method [26].

Transmission electron microscope

GLF were infected FX0910 for 2 h and transfected with either negative control siRNA or ORF022 siRNA. The cells were harvested at 48 hpi and prefixed with 2.5% glutaraldehyde. Subsequently, samples were progressively dehydrated with acetone, permeated with a dehydrating agent, and embedded in Epon-812 embedding agent. After embedding, 60–90 nm ultrathin slices were obtained using an ultrathin microtome. The slices were then stained with uranium acetate for 10 ~ 15 min, and followed by staining with lead citrate for 1 ~ 2 min. Image acquisition of the copper mesh was carried out using JEM-1400FLASH transmission electron microscope.

Transcriptome sequencing analysis

GLF were transfected with pcDNA3.1 or pcDNA3.1-022 for 48 h (group pcDNA3.1-022) and the group pcDNA3.1-022 + FX0910 consisted of GLF transfected pcDNA3.1 or pcDNA3.1-022 for 24 h and then infected with FX0910 for 24 h (Infections were conducted with 10 μl of viral solution per 10^6 cells). Four replicate samples were collected per group. RNA was extracted and sequenced by DNBSEQ-T7 (Biomarker Technologies, Beijing, China). Raw data were quality controlled using fastp and clean reads were mapped to the *Capra hircus* (goat) reference genome (RefSeq assembly accession: GCF_001704415.2) and ORFV reference genome (RefSeq assembly accession: NC_005336.1) using HISAT2 [27]. The expression levels of all mRNA were evaluated using the featureCounts package [28], and the results were reported as fragments per kilobase per million reads (FPKM). Differentially expressed gene analysis (volcano plots, venn diagrams, heatmaps, and KEGG pathway analysis) methods are described in previous research [10]. Gene set enrichment analysis (GSEA) of KEGG gene sets in goats was conducted using the fgsea and ridgeplot packages. Correlation analyses were calculated and visualized using Spearman's method via the cor function and FPKM of viral genes.

ORFV overall alignment rate, differentially expressed genes and correlation analysis

The RNA sequencing reads matched to FX0910 were extracted from the raw data using HISAT2. The extracted data were annotated with featureCounts command (subread software) to obtain the read count of the ORFV genes, and then R was used to calculate the FPKM of the genes. Differentially expressed genes of ORFV were calculated with DESeq2 software and visualised as volcano plots using ggplot2 package. The correlation of ORFV gene expression was calculated from FPKM using the cor function, and genes with an absolute value of correlation with ORF022 greater than 0.9 were visualised using corrplot package.

Statistical analysis

All experiments were performed in triplicates. Statistical analysis was performed using two-tailed student's *t* tests. The results with *P* values less than 0.05 were considered significant.

Results

Genomic features of FX0910 and aFX0910

To characterize genomic changes in attenuated strains, we infected GLF with FX0910 and aFX0910. The cytopathic effect (CPE) were observed at 18 hpi (FX0910) and 48 hpi (aFX0910), characterized by cell rounding and aggregation without detachment. High-quality genomic DNA was extracted during peak CPE and sequenced using next-generation sequencing, yielding complete genome assemblies for both strains, as shown in Fig. 1A. The assembled FX0910 and aFX0910 genomes measured 129,459 bp and 127,372 bp respectively, with a G + C content of 63.9% (Fig. 1B). The sequencing coverage of FX0910 and aFX0910 was 97.5% and 96.78%, respectively, with average depths > 10,000×, ensuring high-confidence assemblies (Fig. 1C). Interestingly, ORFV from Shaanxi presented sequence deletions compared to the reference

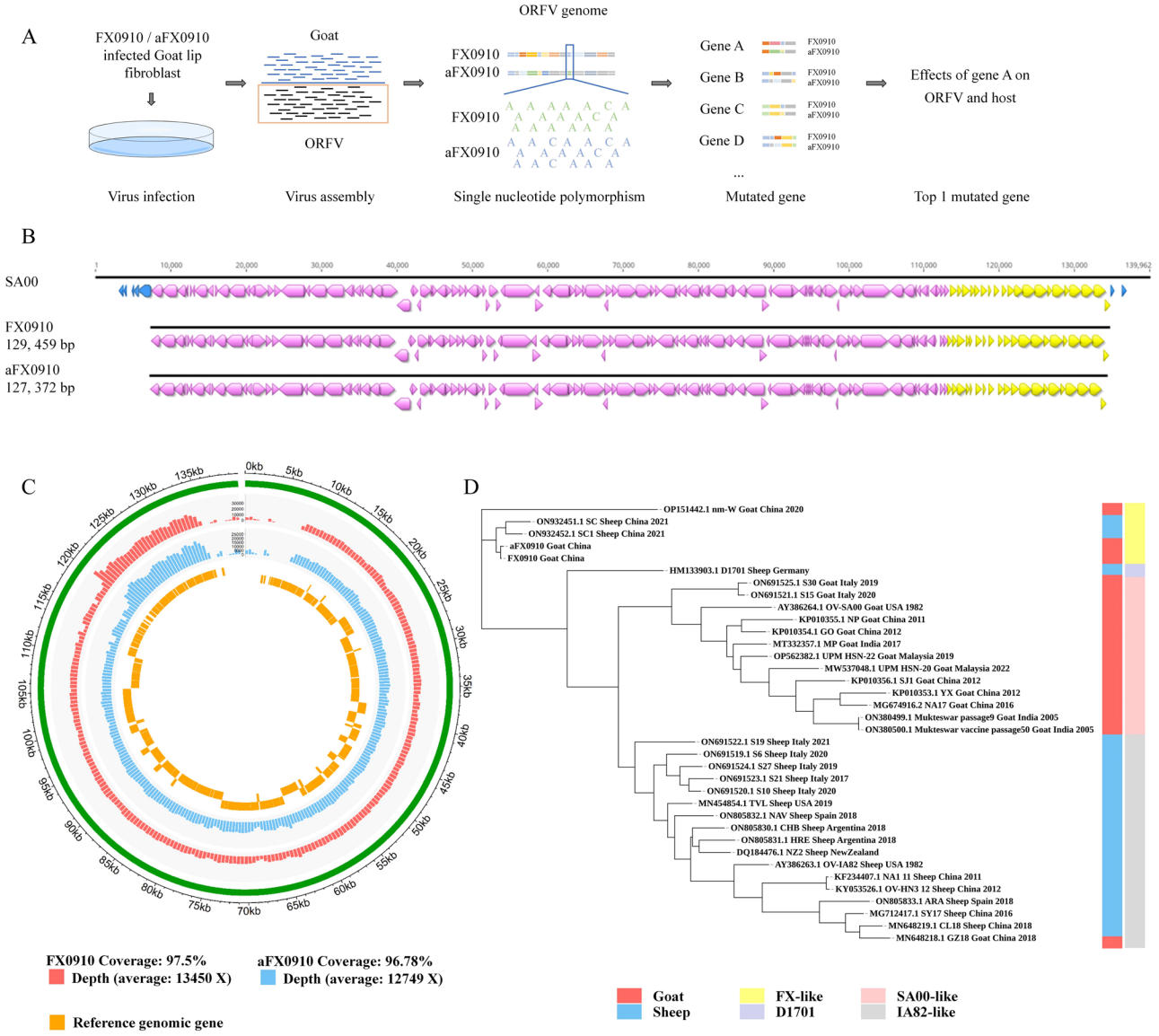

Fig. 1 Whole genome sequencing of two ORFV FX strains. (**A**): Schematic of the WGS approach. (**B**): Genome map of the FX strains. Pink represents the central conserved region, while yellow and blue represent the terminal variant regions, with blue representing genes that are missing. (**C**): Coverage and depth of virus sequencing data. (**D**): Bayesian phylogenetic analysis of published ORFV genomes and FX strain genomes. The posterior probability of all branches in the tree is 100%

genome (SA00 strain) (Fig. 1B-C). The absent sequences include hairpin loops, inverted terminal repeats (ITRs) and seven genes (ORF001, 002, 005, 007, 008, 132, and 134). The sequences of the FX strain correspond to genes ORF009–ORF131 which are the red and yellow regions in Fig. 1B, respectively.

In addition, we performed phylogenetic analysis of the sequences listed in Table S1 (Fig. 1D). The strains were categorized into four clusters: FX-like, D1701, SA00-like, and IA82-like. Despite the different host sources of the FX-like strains, they still clustered together and were closer to the vaccine strain D1701. The posterior probability of all branches in the tree was 100%. Sequence identity results showed that FX strains exhibited greater than 85% sequence similarity to the majority of ORFV isolates (Fig S1A). These results describe the sequence characteristics of the FX strains and demonstrate a close relationship between SC and FX strains.

Mutational events in the aFX0910 compared to FX0910

To explore the attenuation mechanism of aFX0910, we investigated the SNP and INDEL events occurring in it, using the FX0910 genome as a reference. Our analysis identified a total of 103 SNP events with an average mutation frequency of 92.8% (Fig. 2A). Interestingly, only one INDEL mutation was detected - a 23-bp insertion (C

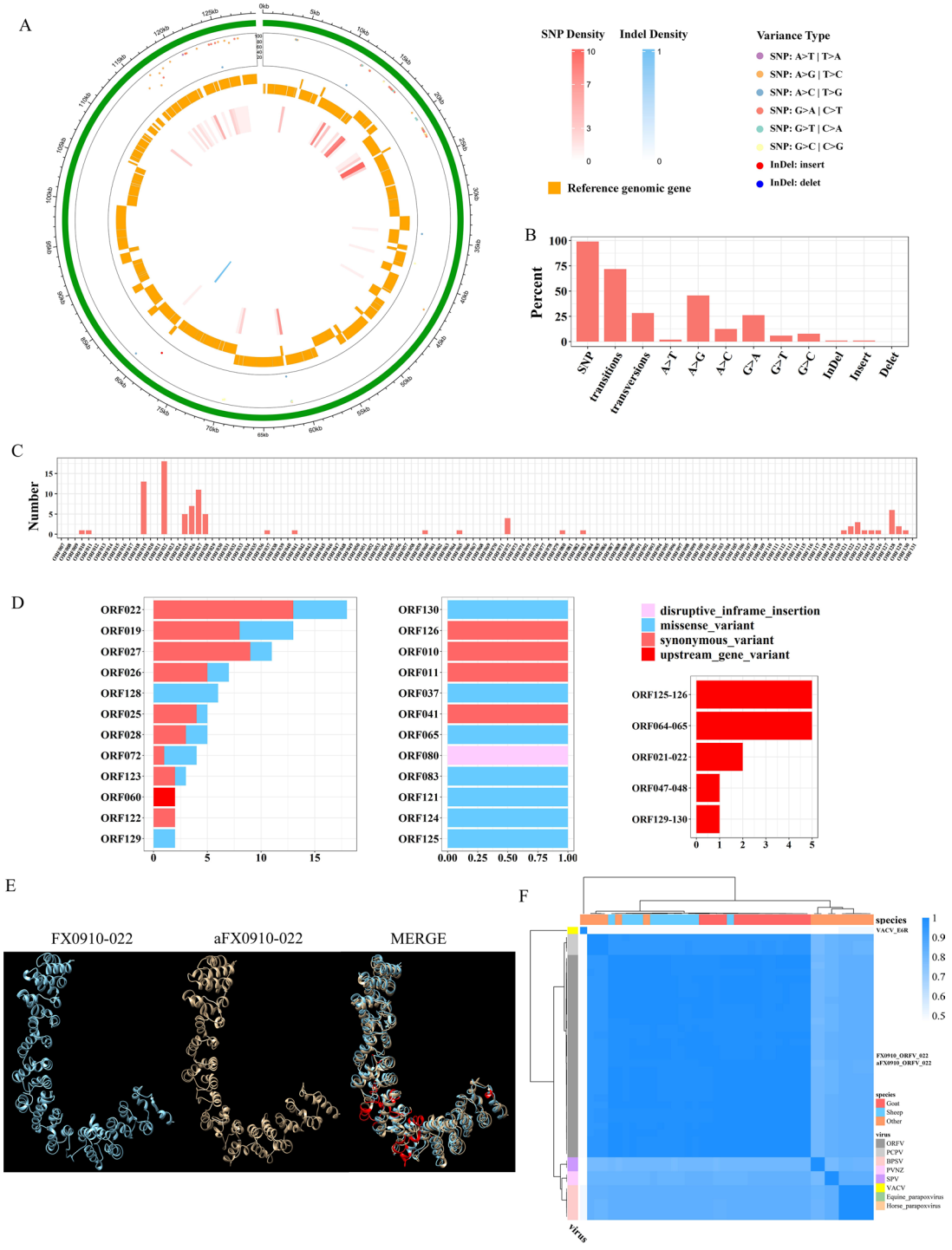

Fig. 2 Single nucleotide polymorphism analysis. (**A**) SNP and INDEL sites and frequencies of aFX0910 compared with FX0910. The green outer circle is FX0910, and the mutation frequency is shown in its inner circle, with different colored dots representing different mutation types and their heights indicating mutation frequencies. The orange circle shows the gene distribution of FX0910, with variant density on the inner side, SNPs in red, and INDELs in blue, where darker colors correspond to a higher number of variants at the position. The legend is on the right side of Figure (**A**. **B**): Percentage statistics for mutation types in the aFX0910 strain. (**C**): Statistics of all mutated genes in the aFX0910 strain. (**D**): Annotation of mutated genes. E: Prediction of the tertiary structure for ORF022. Red indicates differences between FX0910-022 and aFX0910-022. (**F**): Sequence identity analysis of the amino acid sequence of ORF022 and its homologous gene

ACGCGGGGAGCCGGCGCGGGGG) in ORF80. Transitions were approximately three times more common than transversions, with the most frequent events occurring as A > G and G > A (Fig. 2B). Most of the mutated genes were located at termini of the genome (ORF001–ORF028, ORF121–ORF134) (Fig. 2C). Functional annotation of these mutations revealed that synonymous and missense variants were most prevalent (Fig. 2D). Among the 24 mutated genes identified, most remain functionally uncharacterized.

Comparative analysis of FX0910-ORF022 and aFX0910-ORF022 identified five amino acid mutations (Fig. S1B), and changes were observed in the tertiary structure (Fig. 2E). In the secondary structure analysis, an extended strand in FX0910-ORF022 was converted to an α-helix in aFX0910-ORF022 as a consequence of the amino acid mutation at position 501 (Fig. S1C). Phosphorylation site analysis identified differential patterns at positions 276, 497, and 501 between the two strains (Fig. S1D). Nucleotide and amino acid sequences of published ORF022 were collected for phylogenetic analysis, which revealed that ORF022 from FX0910 and aFX0910 were not in the same clade, and ORF022 lacked phylogenetic signal to distinguish between goat and sheep origins (Fig. S1E-F). Sequence identity analysis revealed that ORF022 nucleotide (Fig. S1G) and amino acid (Fig. 2F) homologies were 98–100% and 97.5–100%, respectively. Notably, ORF022 displayed homology to the vaccinia virus E6R gene (Fig. S1H), with 48.5% nucleotide (Fig. S1G) and 48.3% amino acid (Fig. 2F) homology, indicating potential functional similarity. These structural and sequence variations likely contribute to viral attenuation, though their precise mechanistic roles remain to be fully characterized.

ORF022 impacts ORFV replication

The biological properties of ORF022 remain poorly characterized. To gain initial insights, we first examined its subcellular localization, demonstrating predominant cytoplasmic distribution (Fig. 3A). Subsequently, following infection of GLF with an equal copy number of FX0910 and aFX0910 viruses (Fig. S2A), we detected the transcription level of ORF022 at 12, 24, 48, and 72 hpi. We observed an increase in its expression starting at 48 hpi (Fig. 3B-C). In contrast, ORF019 and ORF027 exhibited transcriptional activity at earlier time points, around 6–12 hpi (Fig. S2B-C).

In terms of viral function, we initially explored the relationship between ORF022 and virus replication, revealing a consistent growth trend between ORF022 and ORFV (Fig. 3D-G). Subsequent functional studies demonstrated that ORF022 overexpression significantly increased the relative expression, copy number, virus titer, and protein expression of the virus (Fig. 4A-E). Conversely, inhibition of ORF022 substantially reduced these viral replication markers (Fig. 5A-G). Interestingly, silencing aFX0910-ORF022 did not affect viral transcription or amplification (Fig. S2E-J). Considering the reported involvement of E6R in virion assembly, we investigated the intracellular virus composition following ORF022 inhibition. Electron microscopic observations showed a decrease in mature virions after ORF022 interference, although the virus morphology remained unchanged (Fig. 5H-I). These results suggest that ORF022 affects ORFV replication as a late-expressed protein.

ORF022 inhibits host inflammation-related signaling pathways

However, how ORF022 promotes viral replication and its effects on the host remain unclear. To investigate this, we performed RNA sequencing (RNA-Seq) to analyze host transcriptome changes under two experimental conditions: (i) cells transfected with either pcDNA3.1 or pcDNA3.1-022 for 48 h (pcDNA3.1-022 group), and (ii) cells first transfected with either pcDNA3.1 or pcDNA3.1-022 for 24 h followed by FX0910 infection for an additional 24 h (pcDNA3.1-022 + FX0910 group). Transcriptomic analysis revealed that pcDNA3.1-022 group induced more differentially expressed genes (DEGs) than in the pcDNA3.1-022 + FX0910 group, with a predominance of downregulated genes (Fig. 6A-C). KEGG pathway analysis of DEGs demonstrated significant enrichment in viral infection-related pathways in both groups, including: "Cytokine-cytokine receptor interaction", "TNF signaling pathway", "Viral protein interaction with cytokine and cytokine receptor", and "NF-kappa B signaling pathway" (Fig. 6D-E). GSEA further showed that nearly all these pathways were downregulated (Fig. 6F-G). Signaling pathways related to innate immune response and inflammation, such as "TNF signaling pathway", "IL-17 signaling pathway", "Toll-like receptor signaling pathway", and "JAK-STAT signaling pathway", were significantly down-regulated in pcDNA3.1-022 group. These transcriptomic findings were validated by real-time PCR, confirming the downregulation of inflammation-related genes by ORF022 (Fig. 7A-C).

Subsequent analysis of viral gene expression in the pcDNA3.1-022 + FX0910 group revealed that ORF022 overexpression significantly increased the overall ORFV alignment rate (Fig. 7D). Notably, in addition to ORF022, the expression of ORF112 was also significantly enhanced (Fig. 7E). Correlation analysis of ORFV genes expression (FPKM values) identified ORF123 and ORF016 as showing the strongest co-expression patterns with ORF022 (Fig. 7F). These results suggest that ORF022 suppresses host inflammatory pathways while enhancing viral expression, suggesting its crucial role in

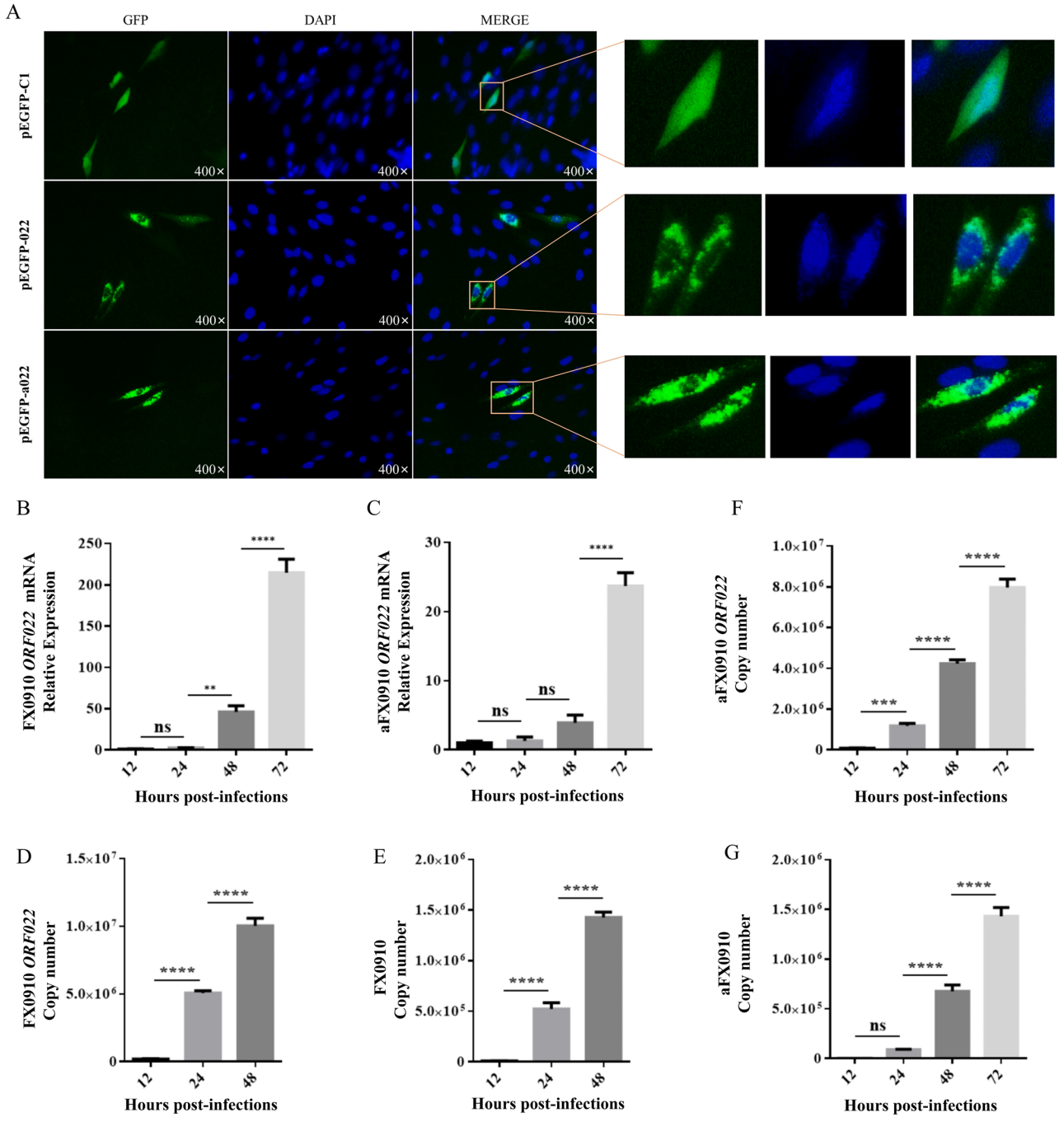

Fig. 3 Subcellular localization and transcriptional dynamics of ORF022. (**A**): Subcellular localization of ORF022. The green fluorescence represents the expression of ORF022 and GFP fusion proteins, while the blue fluorescence indicates the nucleus. B-C: Relative expression of FX0910 (**B**) and aFX0910 (**C**) ORF022 mRNA. GLF was collected at 12, 24, 48, and 72 h after infection with the same viral copy number of FX0910 and aFX0910 viruses, and RNA was extracted to detect ORF022 mRNA. (**D**-**E**): Copy number of FX0910 ORF022 (**D**) and FX0910 (**E**). GLF was collected at 12, 24, and 48 h after infection with FX0910, and DNA was extracted to detect copy number of ORF022 and FX0910. (**F**-**G**): Copy number of aFX0910 ORF022 (**F**) and aFX0910 (**G**). GLF was collected at 12, 24, 48, and 72 h after infection with aFX0910, and DNA was extracted to detect copy number of ORF022 and aFX0910. (**, $P < 0.01$, ***, $P < 0.001$, ****, $P < 0.0001$)

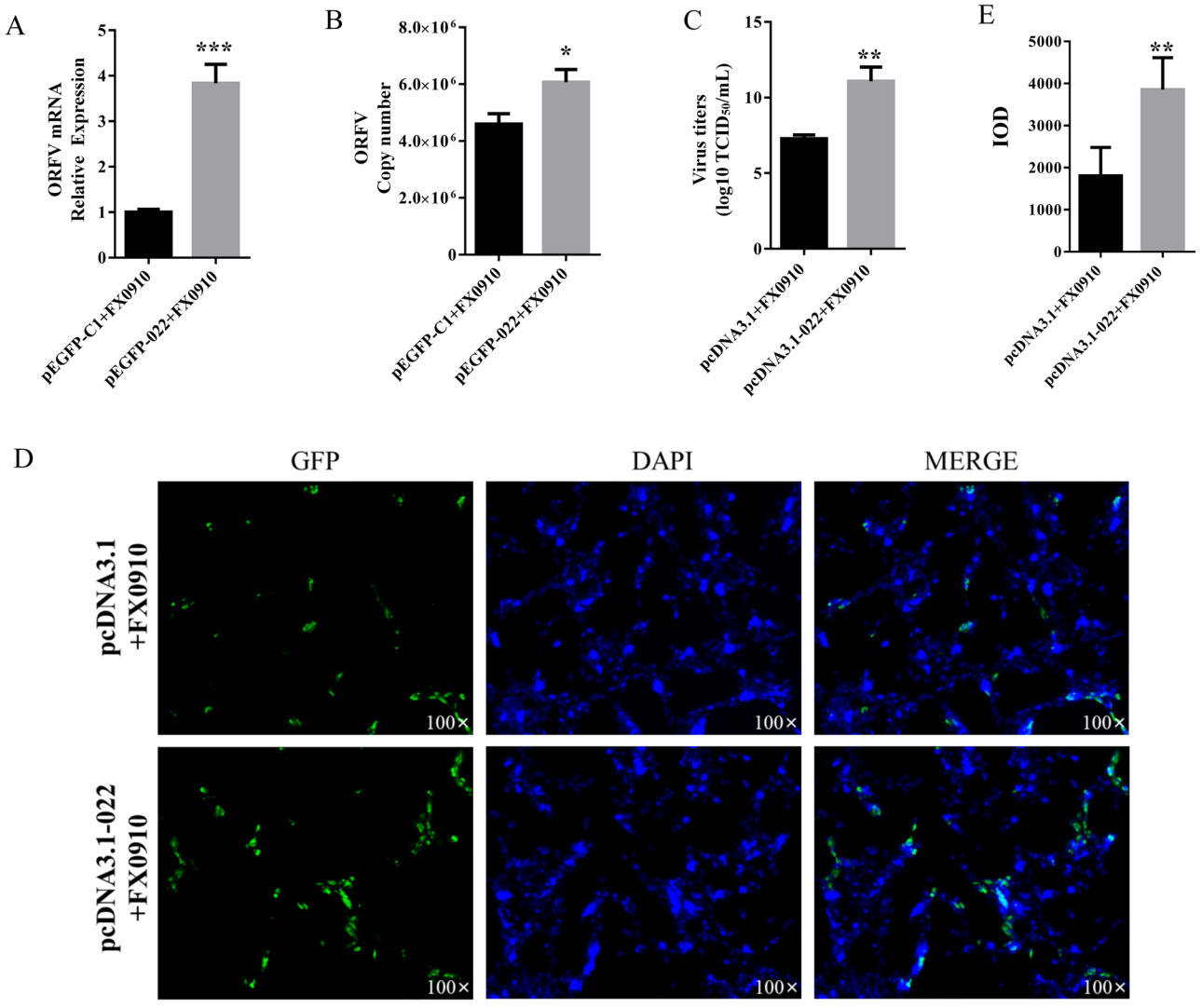

Fig. 4 Effect of overexpressed ORF022 protein on ORFV (FX0910). ORF022 overexpression experiment: GLF were either mock-infected or transfected with pEGFP-022-FX0910 for 24 h and then infected with FX0910 for 24 h. A-B: Real-time analysis of ORFV mRNA (**A**) and copy number (**B**) in ORF022 overexpression experiment. (**C**): $TCID_{50}$ of the cell supernatant in the ORF022 overexpression experiment. (**D**-**E**): Immunofluorescence of ORFV after overexpressing ORF022 (**D**) and Integrated Optical Density analysis (**E**). The green fluorescence represents the expression of ORFV, while the blue fluorescence indicates the nucleus. (*, $P < 0.05$, **, $P < 0.01$, ***, $P < 0.001$)

creating a favorable intracellular environment for ORFV replication.

Discussion

The live attenuated vaccine, a commonly used preventive measure against CE, can effectively prevent ORFV infection [29]. However, the potential risk of reverting to virulence and low efficiency limit its development [9, 30, 31]. Previous studies [10] have indicated that the attenuating strains aFX0910 can suppress the host's innate immune and antiviral responses. Nevertheless, this study focused solely on transcriptional-level effects of FX0910 and aFX0910 on the host, without conducting a comparative analysis of the two FX strains. Mutations in the sequence of the aFX0910 compared with FX0910 may be responsible for the suppression of the innate immune response and the attenuation of FX0910.

This study reports the first complete genome sequence of ORFV isolated in Shaanxi Province, China. Notably, FX0910 (129,459 bp) and aFX0910 (127,372 bp) exhibited shorter genome lengths but showed closest phylogenetic relationship to the longest SC and SC1 strains, implying that successive passages may influence ORFV evolution. The absence of hairpin loops, ITRs and seven genes (ORF001, 002, 005, 007, 008, 132, 134) in the assembled ORFV genome may arise from multiple factors. For instance, technical limitations of short-read sequencing may hinder the accurate resolution of repetitive or GC-rich hairpin loops and ITR regions, leading to incomplete assembly [32, 33]. Additionally, sequencing coverage

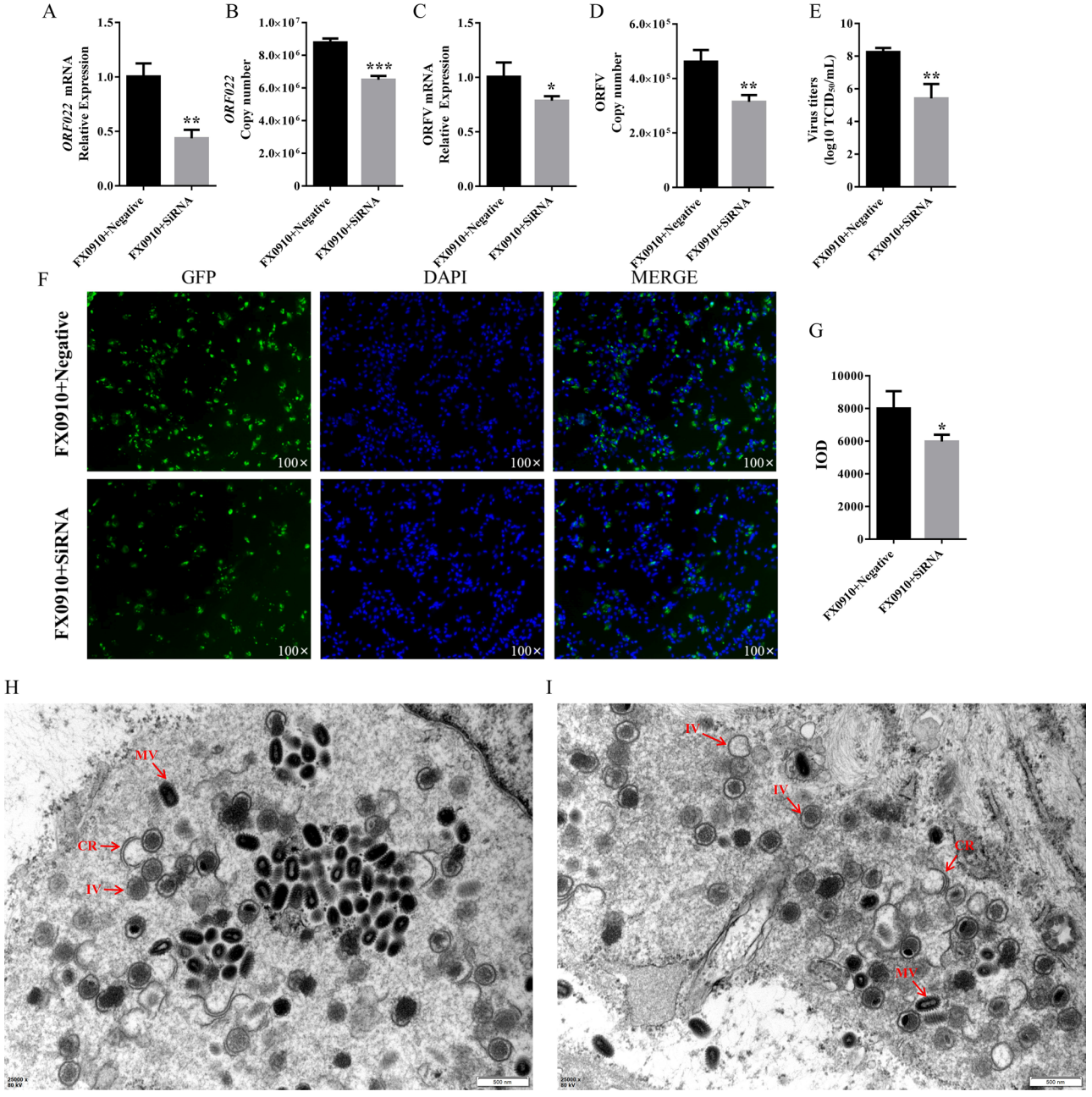

Fig. 5 Effect of interference with ORF022 protein on ORFV (FX0910). ORF022 interference experiment: GLF were infected FX0910 for 2 h and then transfected with either negative siRNA or ORF022 siRNA for 48 h. (**A**-**B**): Real-time analysis of ORF022 mRNA (**A**) and copy number (**B**) in ORF022 interference experiment. (**C**-**D**): Real-time analysis of ORFV mRNA (**C**) and copy number (**D**) in ORF022 interference experiment. (**E**): $TCID_{50}$ of the cell supernatant in the ORF022 interference experiment. (**F**-**G**): Immunofluorescence of ORFV after interference with ORF022 (**F**) and Integrated Optical Density analysis (**G**). The green fluorescence represents the expression of ORFV, while the blue fluorescence indicates the nucleus. (**H**-**I**): Transmission electron microscopy of ORFV, FX0910 infected cells for 2 h and the cells were harvested after 48 h of mock transfection (**H**) or transfection with siRNA (**I**). IV, immature virion, MV, mature virion, CR, crescent. (*, $P < 0.05$, **, $P < 0.01$, ***, $P < 0.001$)

data indicated no or minimal reads aligning to the seven genes, suggesting either strain-specific characteristics or methodological constraints. Further validation using third-generation sequencing is warranted.

To compare the variation between wild-type and attenuated strains and explore the mechanisms underlying FX0910 attenuation, we focused on the SNP events observed between these two strains. The high-frequency mutations of A > G and G > A in ORFV are consistent with the previously reported ADAR- and APOBEC3-driven mutagenesis [34–36]. Additionally, A > G conversion has been observed in varicella vaccines and

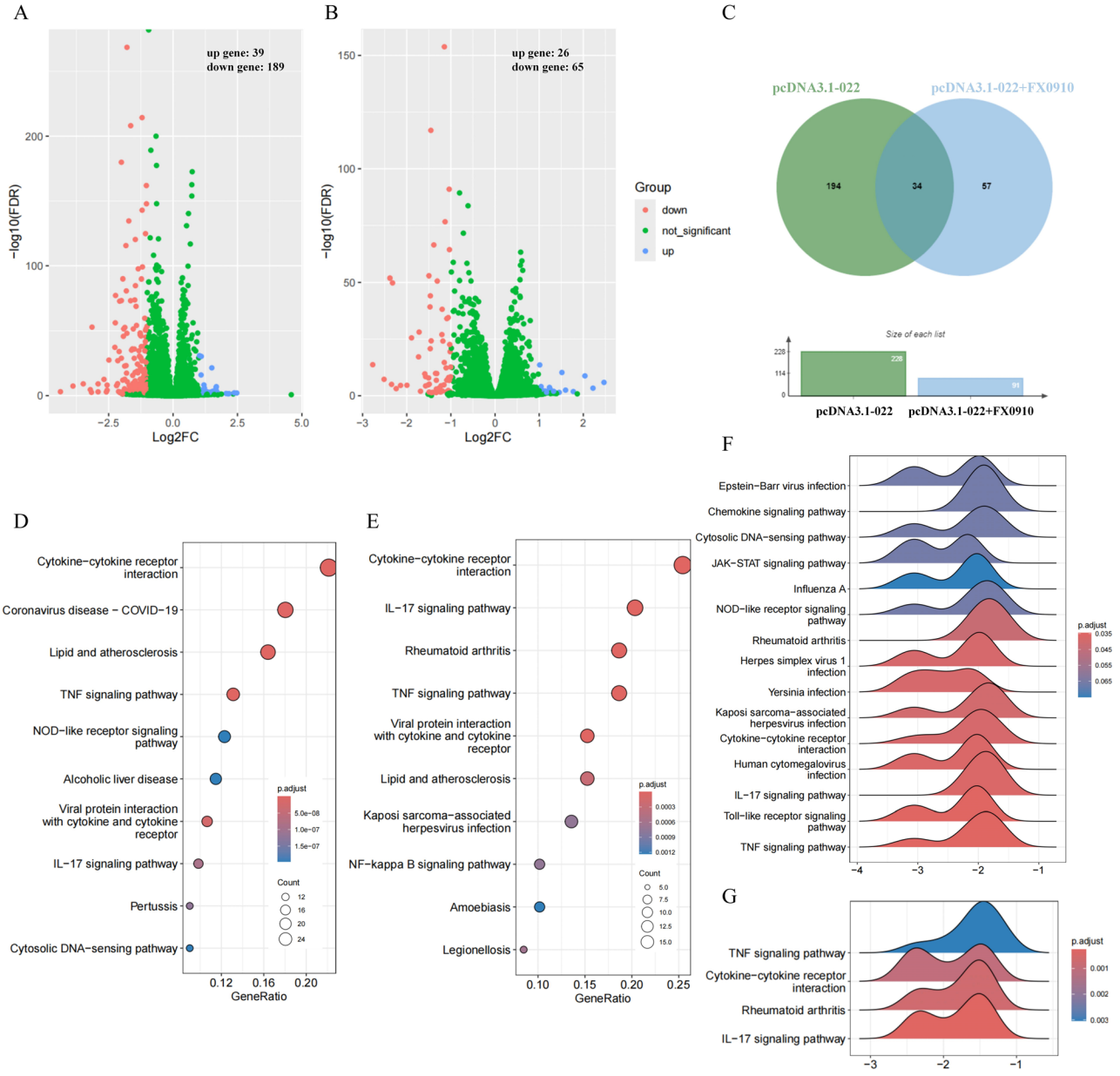

Fig. 6 Differentially expressed genes (DEGs) in ORF022-transfected samples. (**A**-**B**): Volcano plot of DEGs in host cells. Differently expressed genes at 48 h of transfection with ORF022 (group pcDNA3.1-022) (**A**) and 24 h of ORFV infection followed by 24 h of transfection with ORF022 (group pcDNA3.1-022 + FX0910) (**B**). (**C**): Venn diagram of DEGs in pcDNA3.1-022 group and pcDNA3.1-022 + FX0910 group. (**D**-**E**): Top 10 KEGG metabolic pathway enrichment analyses were performed with DEGs in pcDNA3.1-022 group (**D**) and pcDNA3.1-022 + FX0910 group (**E**). (**F**-**G**): GSEA enrichment analyses were performed with DEGs in pcDNA3.1-022 group (**F**) and pcDNA3.1-022 + FX0910 group (**G**)

potentially linked to virulence attenuation [37, 38]. Common mechanisms of vaccine attenuation include single/multiple nucleotide mutations and virulence gene deletions [9]. Our study reveals that most SNPs events were located near the genome termini (ORF001–ORF028, ORF121–ORF134). Interestingly, none of the 24 mutated genes were virulence genes, suggesting that aFX0910 attenuation does not rely on virulence gene alterations. Instead, attenuation may occur through modulation of the host immune response by these mutated genes, either individually or synergistically.

The ORFV genome is large and undergoes base mutations during attenuation [12]. Understanding the functional roles of these mutated genes in viral infection, particularly their impact on replication and host immune responses, is critical for elucidating the mechanism of live attenuated vaccines [39]. In studies of PRRSV, specific mutations in four amino acids were shown to enhance viral cellular adaptation, which may be related

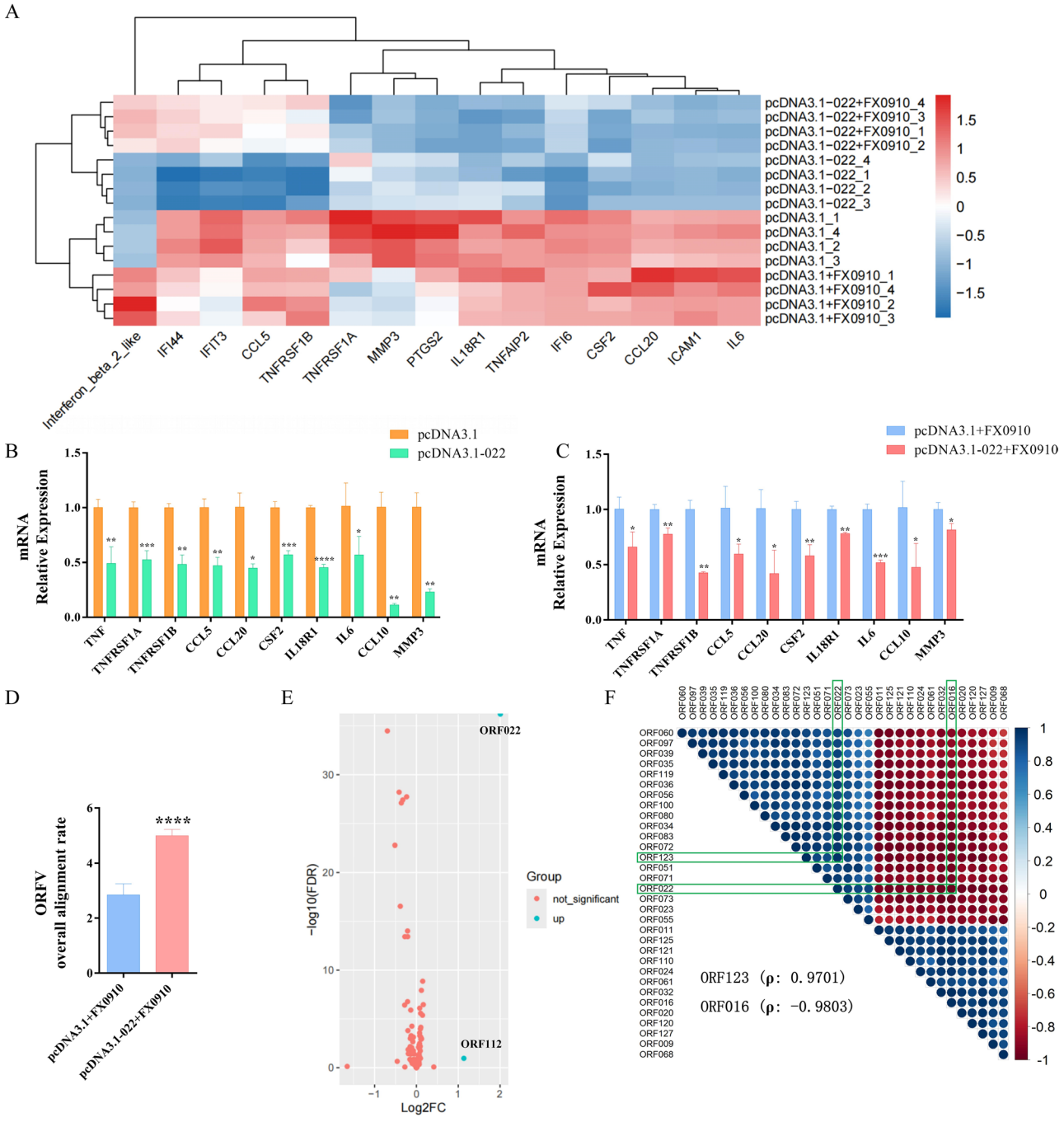

Fig. 7 Expression of inflammation-associated genes and viral genes. A: Heat map of immune and TNF signaling pathway-related genes from pcDNA3.1-022 group and pcDNA3.1-022 + FX0910 group. (**B**-**C**): Real-time PCR of immune and TNF signaling pathway related genes mRNA from pcDNA3.1-022 group (**B**) and pcDNA3.1-022 + FX0910 group (**C**). (**D**): The ratio of reads in the read count (group pcDNA3.1-022 + FX0910) that match FX0910, indexed by FX0910. (**E**): Volcano plot of DEGs in ORFV. (**F**): Spearman correlation analysis of ORFV genes expression (FPKM) with an absolute value of correlation coefficient greater than 0.9 with the ORF022. Red indicates a positive correlation, and blue indicates a negative correlation. (*, $P < 0.05$, **, $P < 0.01$, ***, $P < 0.001$, ****, $P < 0.0001$)

to virulence reversion during reverse passage of attenuated strains [40]. In our study, ORF022 is the gene with the most SNP events, suggesting its potential key role in attenuation. Bioinformatics predictions indicated that mutations at positions 276, 353, and 501 could impact ORF022 function. Furthermore, while ORF022 from FX0910 affected replication of wild-type ORFV, the mutated ORF022 in aFX0910 had no such effect—a disparity likely tied to its amino acid changes. The effect of

amino acid mutations on viral attenuation warrants further investigation.

Previous studies suggested that the ORF022 homologous gene E6R is associated with viral assembly [41, 42], and our transmission electron microscope observations support this finding. To further investigate the function of ORF022, we repeatedly attempted to construct and screen ORF022-knockout ORFV strains via homologous recombination, but the results were not satisfactory. Selection pressure analysis of ORF022 revealed the ω value (dN/dS = 0.0208), indicating negatively selected. This evolutionary constraint suggests ORF022 maintains critical, conserved functions in the viral life cycle [43]. However, the construction of ORF022-deficient recombinant viruses is necessary to investigate the function of ORF022 gene. An inducible system based on the *Escherichia coli lac* operon may be used to construct recombinant viruses [44, 45].

Limited research on ORF022 prompted us to perform RNA-Seq-based gene function prediction. Transcriptomic analysis revealed that ORF022 alone induced a greater number of downregulated host genes compared to its effects during ORFV infection. The Venn diagram demonstrated only 34 overlapping DEGs between the two conditions, indicating that ORF022's function differs when acting alone versus within the viral context. This disparity suggests potential synergistic interactions between ORF022 and other ORFV genes. While interactions among viral genes remain poorly understood, and whether synergy or antagonism among them affects viral infection requires further investigation [46, 47]. GSEA indicated that ORF022 downregulated key innate immune and inflammatory pathways [48–51], including TNF, IL-17, and Toll-like receptor signaling pathway. The relationship between these pathways and ORFV and its genes remains unclear. Notably, ORF022 exerted the most pronounced effect on the TNF signaling pathway, which regulates critical biological processes such as apoptosis, inflammation, and tumorigenesis [52]. The potential inhibition of downstream processes (e.g., NF-κB, JNK, and autophagy) by ORF022 [53–56] may create a favorable environment for viral replication [57], possibly explaining how ORF022 facilitates ORFV accumulation in host cells.

In summary, this study provides genetic information of ORFV wild-type and attenuated strains isolated from goats in Shaanxi province, China, while offering novel insights into the functional role of ORF022 in viral pathogenesis. Our findings reveal significant genomic features of the attenuated aFX0910 strain, elucidate the potential mechanisms underlying its attenuation, and offer insights into the development of novel genetically engineered vaccines.

Conclusions

This study aimed to elucidate the molecular mechanisms underlying attenuation of the ORFV aFX0910 strain. Through comprehensive genomic analysis, we identified 103 distinct SNP events distributed across 24 intragenic and 5 intergenic regions. ORF022, the gene with the highest number of SNPs, was found to modulate viral replication and suppress host inflammatory pathways, as evidenced by transcriptomic profiling. Functional study significantly advances our understanding of how genetic variations in ORF022 contribute to viral attenuation. In summary, the identified SNP events represent a valuable genomic resource for investigating attenuation mechanisms in live attenuated ORFV vaccines. Future analyses of these mutant loci and genes may facilitate the rational design of safer and more effective ORFV vaccines in the future.

Supplementary Information

The online version contains supplementary material available at https://doi.org/10.1186/s12864-025-11663-1.

Supplementary Material 1

Supplementary Material 2

Supplementary Material 3

Supplementary Material 4

Supplementary Material 5

Acknowledgements

The authors are especially thankful to Dr. Xiaoting Yao for her primary cells and virus strains.

Author contributions

T.J. and Y.W. performed all experiments. Y.B, X.C, and S.F. collected and analyzed the data. T.J. and Y.W. drafted the manuscript. Z.N. and D.C. revised the manuscript. X.G. and W.M. conceived and designed the experiments. All authors have read and agreed to the published version of the manuscript.

Funding

Not applicable.

Data availability

Sequence data that support the findings of this study have been deposited in the GenBank with the primary accession code PP943426, PP943427, the RNA-seq data of this study have been deposited in NCBI SRA database (PRJNA1134948).

Declarations

Ethics approval and consent to participate

Not applicable.

Consent for publication

Not applicable.

Competing interests

The authors declare no competing interests.

Received: 23 October 2024 / Accepted: 1 May 2025
Published online: 15 May 2025

References

1. Lawan Z, Bala JA, Bukar AM, Balakrishnan KN, Mangga HK, Abdullah FFJ, et al. Contagious ecthyma: how serious is the disease worldwide? Anim Health Res Rev. 2021;22:40–55.
2. Li S, Jing T, Zhu F, Chen Y, Yao X, Tang X, et al. Genetic analysis of Orf virus (ORFV) strains isolated from goats in China: insights into epidemiological characteristics and evolutionary patterns. Virus Res. 2023;334:199160.
3. Hussain I, Khan MUR, Aslam A, Rabbani M, Masood S, Anjum A. Identification, molecular characterization, and pathological features of Orf virus in sheep and goats in Punjab Province, Pakistan. Trop Anim Health Prod. 2023;55:24.
4. Tryland M, Beckmen KB, Burek-Huntington KA, Breines EM, Klein J. Juang Acta Vet Scand. 2018;60:12.
5. Şevik M, Tryland. Comp Immunol Microbiol Infect Dis. 2019;65:1–6.
6. Kassa T. A review on human Orf: A neglected viral zoonosis. RRTM. 2021;12:153–72.
7. Juang S-J, Win K-T, Chen Y-L, Chen H-W, Cheng P-S. Orf infection on the scalp of a Taiwanese woman: A case report and literature review. Life. 2023;13:358.
8. Bala JA, Balakrishnan KN, Abdullah AA, Mohamed R, Haron AW, Jesse FFA, et al. The re-emerging of Orf virus infection: A call for surveillance, vaccination and effective control measures. Microb Pathog. 2018;120:55–63.
9. Bukar AM, Jesse FFA, Abdullah CAC, Noordin MM, Lawan Z, Mangga HK, et al. Immunomodulatory strategies for parapoxvirus: current status and future approaches for the development of vaccines against Orf virus infection. Vaccines. 2021;9:1341.
10. Yao X, Jing T, Geng Q, Pang M, Zhao X, Li S, et al. Dual analysis of wild-type and attenuated Orf virus and host cell transcriptomes revealed novel virus-host cell interactions. mSphere. 2023. e0039823.
11. Delhon G, Tulman ER, Afonso CL, Lu Z, de la Concha-Bermejillo A, Lehmkuhl HD, et al. Genomes of the parapoxviruses Orf virus and bovine papular stomatitis virus. J Virol. 2004;78:168–77.
12. Du G, Wu J, Zhang C, Cao X, Li L, He J, et al. The whole genomic analysis of the Orf virus strains ORFV-SC and ORFV-SC1 from the Sichuan Province and their weak pathological response in rabbits. Funct Integr Genomics. 2023;23:163.
13. Sonnleitner ST, Sonnleitner S, Hinterbichler E, Halbfurter H, Kopecky DBC, Koblmüller S, et al. The mutational dynamics of the SARS-CoV-2 virus in serial passages in vitro. Virol Sin. 2022;37:198–207.
14. Taher H, Mahyari E, Kreklywich C, Uebelhoer LS, McArdle MR, Moström MJ, et al. In vitro and in vivo characterization of a Recombinant rhesus cytomegalovirus containing a complete genome. PLoS Pathog. 2020;16:e1008666.
15. Bolger AM, Lohse M, Usadel B. Trimmomatic: a flexible trimmer for illumina sequence data. Bioinformatics. 2014;30:2114–20.
16. Li H, Handsaker B, Wysoker A, Fennell T, Ruan J, Homer N, et al. The sequence alignment/map format and samtools. Bioinformatics. 2009;25:2078–9.
17. Li D, Liu C-M, Luo R, Sadakane K, Lam T-W. MEGAHIT: an ultra-fast single-node solution for large and complex metagenomics assembly via succinct de Bruijn graph. Bioinformatics. 2015;31:1674–6.
18. Shumate A, Salzberg SL. Liftoff: accurate mapping of gene annotations. Bioinformatics. 2021;37:1639–43.
19. Quinlan AR, Hall IM. BEDTools: a flexible suite of utilities for comparing genomic features. Bioinformatics. 2010;26:841–2.
20. Gu Z, Gu L, Eils R, Schlesner M, Brors B. Circlize implements and enhances circular visualization in R. Bioinformatics. 2014;30:2811–2.
21. Cingolani P, Platts A, Wang LL, Coon M, Nguyen T, Wang L, et al. A program for annotating and predicting the effects of single nucleotide polymorphisms, SnpEff: SNPs in the genome of Drosophila melanogaster strain w1118; iso-2; iso-3. Fly (Austin). 2012;6:80–92.
22. Katoh K, Misawa K, Kuma K, Miyata T. MAFFT: a novel method for rapid multiple sequence alignment based on fast fourier transform. Nucleic Acids Res. 2002;30:3059–66.
23. Huelsenbeck JP, Ronquist F. MRBAYES: bayesian inference of phylogenetic trees. Bioinformatics. 2001;17:754–5.
24. Pettersen EF, Goddard TD, Huang CC, Couch GS, Greenblatt DM, Meng EC, et al. UCSF Chimera–a visualization system for exploratory research and analysis. J Comput Chem. 2004;25:1605–12.
25. Tang X, Xie Y, Li G, Niyazbekova Z, Li S, Chang J, et al. ORFV entry into host cells via clathrin-mediated endocytosis and macropinocytosis. Vet Microbiol. 2023;284:109831.
26. Biacchesi S, Skiadopoulos MH, Yang L, Murphy BR, Collins PL, Buchholz UJ. Rapid human metapneumovirus microneutralization assay based on green fluorescent protein expression. J Virol Methods. 2005;128:192–7.
27. Kim D, Paggi JM, Park C, Bennett C, Salzberg SL. Graph-based genome alignment and genotyping with HISAT2 and HISAT-genotype. Nat Biotechnol. 2019;37:907–15.
28. Liao Y, Smyth GK, Shi W. FeatureCounts: an efficient general purpose program for assigning sequence reads to genomic features. Bioinformatics. 2014;30:923–30.
29. Lacasta D, Reina R, Ruiz De Arcaute M, Ferrer LM, Benito AA, Tejedor MT, et al. Effect of a topical formulation on infective viral load in lambs naturally infected with Orf virus. VMRR. 2021;12:149–58.
30. Zhao K, He W, Gao W, Lu H, Han T, Li J, et al. Orf virus DNA vaccines expressing ORFV 011 and ORFV 059 chimeric protein enhances immunogenicity. Virol J. 2011;8:562.
31. Martins M, Rodrigues FS, Joshi LR, Jardim JC, Flores MM, Weiblen R, et al. Orf virus ORFV112, ORFV117 and ORFV127 contribute to ORFV IA82 virulence in sheep. Vet Microbiol. 2021;257:109066.
32. Graf A, Rziha H-J, Krebs S, Wolf E, Blum H, Büttner M. Parapoxvirus species revisited by whole genome sequencing: A retrospective analysis of bovine virus isolates. Virus Res. 2024;346:199404.
33. Jain M, Koren S, Miga KH, Quick J, Rand AC, Sasani TA, et al. Nanopore sequencing and assembly of a human genome with ultra-long reads. Nat Biotechnol. 2018;36:338–45.
34. Sun N, Yau SS-T. In-depth investigation of the point mutation pattern of HIV-1. Front Cell Infect Microbiol. 2022;12:1033481.
35. Chen Z, Eggerman TL, Bocharov AV, Baranova IN, Vishnyakova TG, Patterson AP. APOBEC3-induced mutation of the hepatitis virus B DNA genome occurs during its viral RNA reverse transcription into (-)-DNA. J Biol Chem. 2021;297:100889.
36. Isidro J, Borges V, Pinto M, Sobral D, Santos JD, Nunes A, et al. Phylogenomic characterization and signs of microevolution in the 2022 multi-country outbreak of Monkeypox virus. Nat Med. 2022;28:1569–72.
37. Jeon JS, Won YH, Kim IK, Ahn JH, Shin OS, Kim JH, et al. Analysis of single nucleotide polymorphism among Varicella-Zoster virus and identification of vaccine-specific sites. Virology. 2016;496:277–86.
38. Wu Q, Rivailler P, Xu S, Xu W. Comparison of the Whole-Genome sequence of an Oka varicella vaccine from China with other Oka vaccine strains reveals sites putatively critical for vaccine efficacy. J Virol. 2019;93:e02281–18.
39. McGrath ME, Xue Y, Taylor L, Dillen C, Ardanuy J, Gonzalez-Juarbe N, et al. SARS-CoV-2 ORF8 modulates lung inflammation and clinical disease progression. PLoS Pathog. 2024;20:e1011669.
40. Wang J, Zhang M, Cui X, Gao X, Sun W, Ge X, et al. Attenuated Porcine reproductive and respiratory syndrome virus regains its fatal virulence by serial passaging in pigs or Porcine alveolar macrophages to increase its adaptation to target cells. Microbiol Spectr. 2022;10:e0308422.
41. Boyd O, Turner PC, Moyer RW, Condit RC, Moussatche N. The E6 protein from vaccinia virus is required for the formation of immature virions. Virology. 2010;399:201–11.
42. Resch W, Weisberg AS, Moss B. Expression of the highly conserved vaccinia virus E6 protein is required for virion morphogenesis. Virology. 2009;386:478–85.
43. Scarpa F, Sernicola L, Farcomeni S, Ciccozzi A, Sanna D, Casu M, et al. Phylodynamic and evolution of the hemagglutinin (HA) and neuraminidase (NA) genes of influenza A(H1N1) pdm09 viruses Circulating in the 2009 and 2023 seasons in Italy. Pathogens. 2024;13:334.
44. Zhang YF, Moss B. Inducer-dependent conditional-lethal mutant animal viruses. Proc Natl Acad Sci U S A. 1991;88:1511–5.
45. Ward GA, Stover CK, Moss B, Fuerst TR. Stringent chemical and thermal regulation of Recombinant gene expression by vaccinia virus vectors in mammalian cells. Proc Natl Acad Sci U S A. 1995;92:6773–7.
46. Brady J, Khoury G. Trans activation of the Simian virus 40 late transcription unit by T-antigen. Mol Cell Biol. 1985;5:1391–9.
47. Fossum E, Friedel CC, Rajagopala SV, Titz B, Baiker A, Schmidt T, et al. Evolutionarily conserved herpesviral protein interaction networks. PLoS Pathog. 2009;5:e1000570.
48. Li M, Li Y, Liu Y, Li X, Lao S, Long Z, et al. The Epstein-Barr virus small capsid protein BFRF3 disrupts the NF-κB signaling pathway by inhibiting p65 activity. FASEB J. 2024;38:e23820.
49. Chen Q, Pan X-H, Wang Q-H, Bai J-J, Jiang L-Q, Li Y-H, et al. Sophora subprostrate polysaccharide targets LncRNA MSTRG.5823.1 to suppress PCV2-mediated immunosuppression via TNF/NF-κB signaling. Int Immunopharmacol. 2024;139:112701.
50. Wang F, Tang Y-S, Cao F, Shou J-W, Wong C-K, Shaw P-C. 3,4,5-tri-O-caffeoylquinic acid attenuates influenza A virus induced inflammation

through Toll-like receptor 3/7 activated signaling pathway. Phytomedicine. 2024;132:155896.
51. Liu J, Li B, Zhou X, Liu G, Li C, Hu Z, et al. Uncovering the mechanisms of Zhubi Decoction against rheumatoid arthritis through an integrated study of network pharmacology, metabolomics, and intestinal flora. J Ethnopharmacol. 2025;336:118736.
52. Chen G, Goeddel DV. TNF-R1 signaling: a beautiful pathway. Science. 2002;296:1634–5.
53. Zheng Y, Li S, Li S-H, Yu S, Wang Q, Zhang K, et al. Transcriptome profiling in swine macrophages infected with African swine fever virus at single-cell resolution. Proc Natl Acad Sci U S A. 2022;119:e2201288119.
54. Kung P-L, Chou T-W, Lindman M, Chang NP, Estevez I, Buckley BD, et al. Zika virus-induced TNF-α signaling dysregulates expression of neurologic genes associated with psychiatric disorders. J Neuroinflammation. 2022;19:100.
55. Liniger M, Gerber M, Renzullo S, García-Nicolás O, Ruggli N. TNF-Mediated Inhibition of classical swine fever virus replication is IRF1-, NF-κB- and JAK/STAT Signaling-Dependent. Viruses. 2021;13:2017.
56. Santos LD, Antunes KH, Muraro SP, de Souza GF, da Silva AG, de Felipe J. TNF-mediated alveolar macrophage necroptosis drives disease pathogenesis during respiratory syncytial virus infection. Eur Respir J. 2021;57:2003764.
57. Li J-Y, Liao C-H, Wang Q, Tan Y-J, Luo R, Qiu Y, et al. The ORF6, ORF8 and nucleocapsid proteins of SARS-CoV-2 inhibit type I interferon signaling pathway. Virus Res. 2020;286:198074.

Publisher's note